Critical differences in HIV-1 and HIV-2 protease specificity for clinical inhibitors

Yunfeng Tie,[1] Yuan-Fang Wang,[1] Peter I. Boross,[2] Ting-Yi Chiu,[1] Arun K. Ghosh,[3] Jozsef Tozser,[2] John M. Louis,[4] Robert W. Harrison,[1,5] and Irene T. Weber[1,6]*

[1] Department of Biology, Georgia State University, Atlanta, Georgia 30303

[2] Faculty of Medicine, Department of Biochemistry and Molecular Biology, University of Debrecen, Debrecen, Hungary

[3] Department of Chemistry and Medicinal Chemistry, Purdue University, West Lafayette, Indiana 47907

[4] Laboratory of Chemical Physics, National Institute of Diabetes and Digestive and Kidney Diseases, National Institutes of Health, DHHS, Bethesda, Maryland 20892-0520

[5] Department of Computer Science, Georgia State University, Atlanta, Georgia 30303

[6] Department of Chemistry, Georgia State University, Atlanta, Georgia 30303

Received 25 October 2011; Revised 13 December 2011; Accepted 13 December 2011
DOI: 10.1002/pro.2019
Published online 11 January 2012 proteinscience.org

Abstract: Clinical inhibitor amprenavir (APV) is less effective on HIV-2 protease (PR_2) than on HIV-1 protease (PR_1). We solved the crystal structure of PR_2 with APV at 1.5 Å resolution to identify structural changes associated with the lowered inhibition. Furthermore, we analyzed the PR_1 mutant (PR_{1M}) with substitutions V32I, I47V, and V82I that mimic the inhibitor binding site of PR_2. PR_{1M} more closely resembled PR_2 than PR_1 in catalytic efficiency on four substrate peptides and inhibition by APV, whereas few differences were seen for two other substrates and inhibition by saquinavir (SQV) and darunavir (DRV). High resolution crystal structures of PR_{1M} with APV, DRV, and SQV were compared with available PR_1 and PR_2 complexes. Val/Ile32 and Ile/Val47 showed compensating interactions with SQV in PR_{1M} and PR_1, however, Ile82 interacted with a second SQV bound in an extension of the active site cavity of PR_{1M}. Residues 32 and 82 maintained similar interactions with DRV and APV in all the enzymes, whereas Val47 and Ile47 had opposing effects in the two subunits. Significantly diminished interactions were seen for the aniline of APV bound in PR_{1M} and PR_2 relative to the strong hydrogen bonds observed in PR_1, consistent with 15- and 19-fold weaker inhibition, respectively. Overall, PR_{1M} partially replicates the specificity of PR_2 and gives insight into drug resistant mutations at residues 32, 47, and 82. Moreover, this analysis provides a structural explanation for the weaker antiviral effects of APV on HIV-2.

Keywords: HIV/AIDS; drug resistance; aspartic protease; antiviral inhibitors; molecular recognition

Introduction

Acquired immunodeficiency syndrome (AIDS) is a major health challenge with a global estimate of over 30 million people infected with HIV and 1.8 million deaths in 2009.[1] Anti-retroviral treatment has increased survival of HIV-infected patients, however, long-term therapy is compromised by the selection of drug resistance mutations and the high genetic diversity of the virus. There are two major types: HIV-1 and HIV-2; the more common HIV-1 is subdivided into the four groups of M, N, O, and P as well as several subtypes. HIV-2 infections account for more

Abbreviations: AIDS, acquired immunodeficiency syndrome; APV, amprenavir; DRV, darunavir; HAART, Highly Active Antiretroviral Therapy; HIV-1, human immunodeficiency virus type 1; HIV-2, human immunodeficiency virus type 2; IDV, indinavir; PI, protease inhibitor; PR, HIV protease; PR_1: HIV-1 protease; PR_1M: HIV-1 protease with V32I, I47V and V82I mutations; PR_2: HIV-2 protease; RMSD, root mean square deviation; SQV, saquinavir; THF, tetrahydrofuran.

**Correspondence to:* Irene T. Weber, Department of Biology, Georgia State University, P.O. Box 4010, Atlanta, GA 30302-4010. E-mail: iweber@gsu.edu

than 1 million people, or about a third of the HIV prevalence in West Africa[2,3] and are spreading into other continents.[4,5] Treatment of HIV-2 infections employs the drugs developed for HIV-1, however, several drugs are less effective on HIV-2.[2,3] A further therapeutic quandary is posed by the drug resistant mutations arising in HIV-2 and co-infections of HIV-1 and HIV-2.[2,6]

HIV-1 protease (PR_1) is a very effective drug target for AIDS treatment because its activity is essential for hydrolyzing the viral Gag and Gag-Pol precursor polyproteins during the maturation of infectious virus.[7] PR_1 inhibitors illustrate the success of structure-guided drug designs. Several hundred crystal structures are available for wild type and mutant PR_1 complexes with the clinical drugs and many other inhibitors.[8] Currently, nine FDA approved PR_1 inhibitors are used in Highly Active Antiretroviral Therapy (HAART). Some of these clinical inhibitors, such as amprenavir (APV) and nelfinavir (NFV), show lower efficacy on HIV-2 infections and weaker inhibition of HIV-2 protease (PR_2).[2,7,9] PR_1 and PR_2 share 39–48% amino acid sequence identity depending on the strain of virus and similar overall structure.[3,10–12] The two enzymes differ in their cleavage site sequences in the viral precursors and in their specificity for peptide substrates and inhibitors, especially at the P2 positions of peptide substrates.[13,14] The sequence differences between PR_1 and PR_2 are expected to be responsible for the differences in efficacy of inhibitors and include substitutions observed in resistance of HIV-1 to the current drugs (Fig. 1).[15] In particular, the binding site for clinical inhibitors differs only in the conservative substitution of hydrophobic residues Val32, Ile47, and Val82 in PR_1 by Ile32, Val47, and Ile82 in PR_2. Earlier studies showed that PR_1 bearing the substitutions, V32I, I47V, and V82I, altered the inhibition but not the binding mode of a tripeptide inhibitor.[16,17] These residues are the sites of drug resistance mutations V32I, I47V, and various substitutions of Val82 in HIV-1 (Fig. 1).[15]

In contrast to PR_1, very few crystal structures are available for PR_2 complexes with clinical inhibitors. We have shown that DRV, which maintains antiviral potency on HIV-1 and HIV-2 infections, demonstrates similar binding mode in PR_1 and PR_2 crystal structures, as does indinavir (IDV).[11,12] Here, we report the crystal structure of PR_2 with APV, which by comparison with our PR_1–APV structure[18] helps explain the lower efficacy of this inhibitor on HIV-2 infections. Furthermore, we constructed the PR_1 mutant with substitutions of the three PR_2 residues that differ in the inhibitor-binding site (V32I, I47V, and V82I; designated PR_{1M}) to investigate the importance of these residues in the substrate specificity and binding of clinical inhibitors. The inhibitors APV, DRV and SQV were selected due to their distinct effects on the two types of virus. HIV-2 strains were shown to be susceptible to DRV[19] and to SQV,[20,21] while natural resistance to APV was found for several HIV-2 strains.[20–22] Thus, crystallographic and kinetic analysis of PR_{1M}, PR_1 and PR_2 will improve our understanding of the differences in inhibitor potency. Furthermore, this knowledge can be exploited in the design of broader-spectrum inhibitors targeting the natural variants of PR_1, PR_2 and their drug resistant mutants.

Results

Substrate specificity and inhibition

The three enzymes were assessed for hydrolysis of peptides representing natural cleavage sites of HIV-2 precursor polyproteins. Also, peptides were tested with variants of the P2 and P4 positions of the HIV-1 MA-CA cleavage site (between the MA and CA proteins in the precursor) that distinguish the substrate specificities of retroviral PRs.[14,23] Two peptides represent the HIV-2 cleavage sites CA/p2 (KARLM↓AEALK, where ↓ indicates the position of the cleaved peptide bond) and p2/NC (IPFAA↓AQQRK). Four peptides were selected with different amino acids (Val and Leu) at the P2 and P4 positions in the HIV-1 MA/CA cleavage site (VSQNY↓PIVQ) to explore the variation due to the substitutions of residues 32, 47, and 82 that differ in the substrate binding cavities of PR_1 and PR_2 (Fig. 1). Kinetic parameters are summarized in Table I. The K_m values showed low variation ranging from 0.07 to 0.57 m*M* over the measured PRs and substrates. Significant differences were observed only for hydrolysis of the HIV-2 p2/NC peptide where the K_m values were identical for PR_{1M} and PR_2 and 4-fold lower than that for PR_1. The k_{cat} values for different substrates exhibited a wider range covering two orders of magnitude from 0.06 to 5.1 s^{-1}. Values of k_{cat} for PR_{1M} were closer to those of PR_2 for substrates (2), (4), and (6), however, the three PRs had k_{cat} values in the same range for substrates (1) and (3).

The k_{cat}/K_m value is the most useful for comparing the specificity of different enzymes. PR_2 had significantly greater catalytic efficiency by 5- to 10-fold compared to PR_1 for substrates (1), (2), (4), and (6). Similarly, PR_{1M} mutant showed 2.6–15-fold higher k_{cat}/K_m values relative to PR_1. PR_{1M} and PR_2 shared similar k_{cat}/K_m values for substrate (2) representing the HIV-2 p2/NC site and substrate (6). However, PR_{1M} showed k_{cat}/K_m values intermediate between the values for PR_1 and PR_2 for substrates (1) and (4). The three enzymes had indistinguishable k_{cat}/K_m values (less than two-fold difference) for substrates (3) and (5). The PR_{1M} mutant showed no preference for the Val or Leu at P2 in peptides (3) and (4),

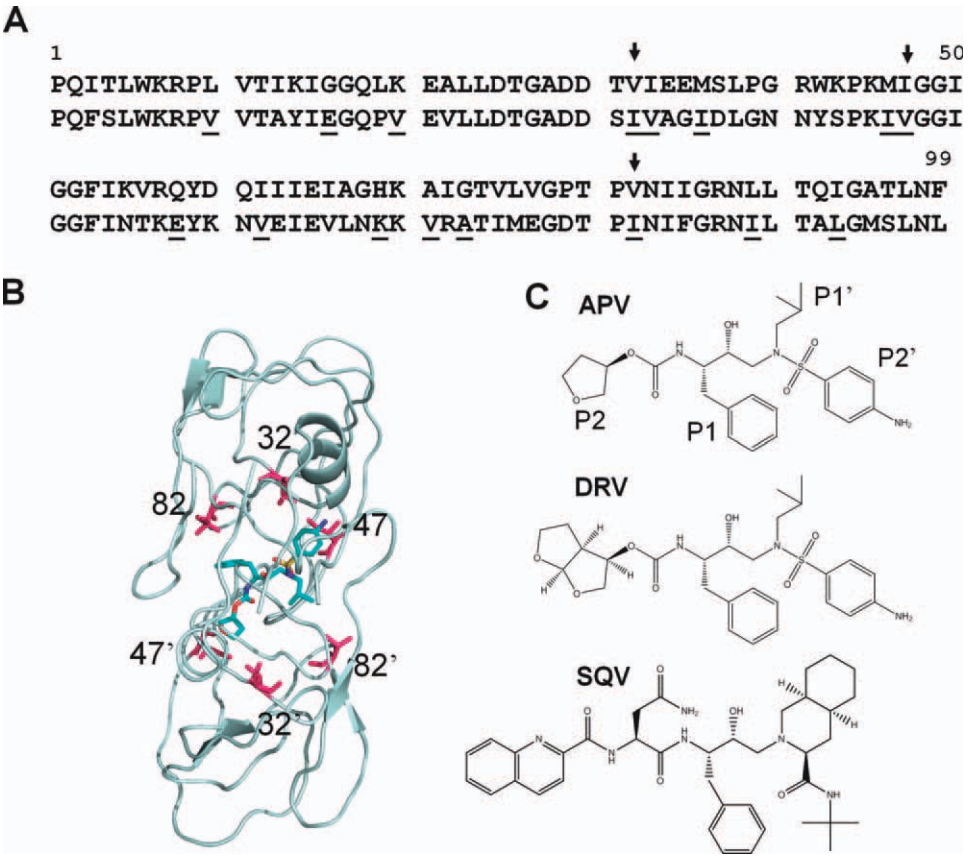

Figure 1. A: Amino acid sequences of HIV PR_1 (upper line) and PR_2 (lower line). PR_2 residues associated with drug resistance in PR_1 are underlined. Arrows indicate the amino acid differences in the inhibitor binding site Val/Ile32, Ile/Val47, and Val/Ile82. B: Location of residues 32, 47, and 82 (magenta) in PR dimer with SQV (cyan). C: Chemical structures of APV, DRV, and SQV with groups P2-P2′ labeled for APV. [Color figure can be viewed in the online issue, which is available at wileyonlinelibrary.com.]

although P2 Leu was favored by PR_2 and Val by PR_1. Leu at the P4 position was preferred over Val in peptides (5) and (6) for PR_2 and PR_{1M}, although the opposite trend was observed for PR_1. Overall, the kinetic parameters of PR_{1M} mutant were more comparable to those of PR_2 rather than PR_1.

Table I. *Kinetic Parameters Obtained for Oligopeptide Substrates*

	Peptide	Protease	K_m (mM)	k_{cat} (s^{-1})	k_{cat}/K_m ($mM^{-1}s^{-1}$)	Relative k_{cat}/K_m
(1) HIV-2 CA/p2	KARLM↓AEALK	PR_1[a]	0.13	0.3	2.3	1.0
		PR_2[a]	0.08	1.2	15.0	6.5
		PR_{1M}	0.09	0.6	6.6	2.9
(2) HIV-2 p2/NC	IPFAA↓AQQRK	PR_1[a]	0.28	0.3	1.1	1.0
		PR_2[a]	0.07	0.8	11.4	10.4
		PR_{1M}	0.07	1.2	16.3	14.8
(3) HIV-1 MA/CA	VSQ**V**Y↓PIVQ	PR_1	0.24	2.6	10.8	1.0
		PR_2[b]	0.43	2.5	5.8	0.5
		PR_{1M}	0.35	3.0	8.6	0.8
(4) HIV-1 MA/CA	VSQ**L**Y↓PIVQ	PR_1[b]	0.12	0.4	3.3	1.0
		PR_2[b]	0.17	3.4	20.0	6.1
		PR_{1M}	0.38	5.1	8.6	2.6
(5) HIV-1 MA/CA	V**V**QNY↓PIVQ	PR_1	0.19	0.16	0.8	1.0
		PR_2[c]	N.D.	N.D.	0.6	0.8
		PR_{1M}	0.23	0.18	0.8	1.0
(6) HIV-1 MA/CA	V**L**QNY↓PIVQ	PR_1[c]	0.40	0.06	0.2	1.0
		PR_2[c]	0.57	0.6	1.0	5.0
		PR_{1M}	0.32	0.26	0.8	4.0

[a] Data taken from Reference 35.
[b] Data taken from Reference 13.
[c] Data taken from Reference 48.
Residues that were substituted in the HIV-1 MA/CA cleavage site VSQNY↓PIVQ are in bold and underlined.

Table II. *K_i Values for Inhibitors (nM)*

	DRV	SQV	APV
PR_1	0.04	0.11	0.17
PR_{1M}	0.23 (6)	0.24 (2)	2.53 (15)
PR_2	0.04 (1)	0.07 (0.6)	3.24 (19)

Values relative to PR_1 are shown in parentheses.

The catalytic activities of the HIV proteases were inhibited by APV, DRV and SQV (Table II). The results for PR_1 and PR_2 are similar to those reported using a chromogenic substrate based on the HIV-1 CA-p2 site.[9] APV exhibited good inhibition for PR_1 while PR_{1M} and PR_2 were more poorly inhibited with K_i values of 15 and 19-fold higher than for PR_1, respectively. DRV showed similar inhibition for PR_1 and PR_2, and 6-fold weaker inhibition of the mutant. SQV showed similar inhibition constants for all three enzymes with differences of no more than 2-fold. Both SQV and DRV retain antiviral potency for HIV-2 and HIV-1 infections. Overall, APV is the least effective among three inhibitors for PR_{1M} and PR_2, which is consistent with the observations of natural resistance of HIV-2 to APV, and the 10-30 fold higher IC_{50} values of APV for HIV-2 infected compared to HIV-1 infected cells.[3,21]

Crystallographic analysis

Crystal structures were solved for the PR_2 with APV and of PR_{1M} complexes with clinical inhibitors DRV, SQV, and APV (Table III). The asymmetric units contained one PR dimer with residues numbered 1–99 and 1′–99′. Three datasets were collected with high resolutions of 1.26–1.51 Å and were refined to final R-factors of 0.16–0.18. The PR_{1M}-SQV complex had the lowest resolution of 1.88 Å and was refined to an R-factor of 0.19. Clear electron density was observed for all the residues in PR_{1M} and PR_2, inhibitor, solvent molecules and ions in all structures. The APV complex showed a single conformation of inhibitor in both PR_{1M} and PR_2, although the P2′ aniline group had two alternate positions in PR_{1M} (Fig. 2). Two alternate orientations of DRV were refined in the active site cavity of PR_{1M}-DRV, as described previously.[24] An extra SQV molecule was observed in an extension of the usual binding site in the structure of PR_{1M}-SQV, as described later. The crystal structure of PR_{1M}-APV, obtained from crystals grown in potassium iodine solution, was refined with 21 iodide ions, while one sodium and two chloride ions were observed in the PR_{1M}-DRV crystals grown with sodium chloride as precipitant. Iodide ions were identified by the high peaks in electron density maps, even at partial occupancy, abnormal B factors, and van der Waals contacts of 3.4–3.8 Á to nitrogen atoms, as noted in Reference [18]. The solvent in the PR_2-APV structure comprised one sodium, eight chloride, seven zinc ions, and six imidazole molecules from the crystallization solution, as described for PR_2-DRV.[12]

Second binding site for SQV in PR_{1M}-SQV

The structure of PR_{1M} in complex with SQV contained an extra SQV molecule (designated SQV-B) bound in an extension of the regular inhibitor binding pocket. This second SQV binding site has not

Table III. *Crystallographic Data Collection and Refinement Statistics*

Structures	PR_{1M}-DRV	PR_{1M}–SQV	PR_{1M}-APV	PR_2-APV
Space group	$P2_12_12$	$P2_12_12_1$	$P2_12_12$	C2
Unit cell parameters				
a (Å)	58.6	29.2	58.4	106.0
b (Å)	86.2	67.4	86.6	31.0
c (Å)	46.2	92.8	46.3	56.2
β (°)	90.0	90.0	90.0	91.66
Resolution range (Å)	50–1.42	50–1.88	50–1.26	50–1.51
Unique reflections	45,155	15,355	58,771	25,917
R_{merge} (%) overall (final shell)	8.4 (33.6)	10.8 (40.8)	6.3 (36.1)	8.1 (25.5)
$I/\sigma(I)$ overall (final shell)	16.2 (3.0)	13.7 (2.2)	14.5 (2.1)	12.8 (2.9)
Completeness (%) overall (final shell)	90.9 (50.5)	98.3 (87.5)	91.3 (59.9)	90.3 (63.3)
Data range for refinement (Å)	10–1.42	10–1.88	10–1.26	10–1.51
R (%)	15.7	18.8	15.9	18.2
R_{free} (%)	20.8	23.4	19.1	23.8
No. of solvent atoms (total occupancies)	178 (138.3)	100 (83.0)	162 (103.5)	144 (124.7)
RMS deviation from ideality				
Bonds (Å)	0.010	0.032	0.012	0.008
Angle distance (Å)	0.030	2.388*	0.031	0.027
Average B-factors (Å^2)				
Main-chain atoms	17.8	17.3	17.0	17.7
Side-chain atoms	24.3	22.5	23.8	23.0
Inhibitor	15.6	19.5	17.5	20.8
Solvent	27.9	20.3	24.6	24.6

* RMS deviation in °

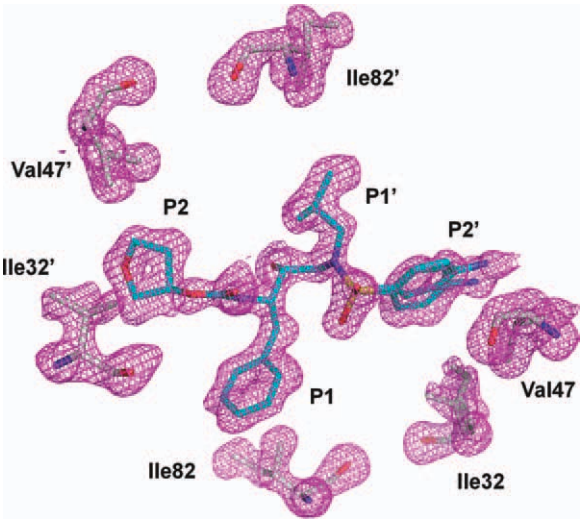

Figure 2. Omit electron density map for APV and mutated residues Ile32, Val47, and Ile82 in the two subunits of the PR_{1M} dimer. The map was contoured at 2.2σ level. Ile82 and 82′ in the S1/S1′ subsites interact with P1′ and P1 groups of the inhibitor. Ile32/32′ and Val47/47′ contribute to the S2/S2′ subsites and interact with the P2 and P2′ groups of APV. [Color figure can be viewed in the online issue, which is available at wileyonlinelibrary.com.]

been reported before. The P3 quinoline of SQV-B interacted with the aromatic P3 and P1 groups of SQV-A bound in the usual position in the active site cavity [Fig. 3(A)]. Hence, the SQV molecules alternate their orientation continuously though the adjacent binding pockets of the PR dimers packed in the crystal lattice [Fig. 3(B)]. Half of SQV-B interacted with the PR_{1M} dimer while the other half interacted with two symmetry related dimers [Fig. 3(C)]. SQV-B formed a hydrogen bond with the side chain of Glu34′, a water-mediated interaction with the side chain of Arg8′, and hydrophobic interactions with Leu10′, Glu21′, Leu23′, Pro81′, and Ile82′. The residues Arg8, Pro81, Ile82, Gly48′, and Phe53′ from symmetry dimer 1 and Trp42, Pro44 from symmetry dimer 2 formed a binding site for the other part of SQV-B. Two direct hydrogen bonds were formed between SQV-B oxygen atoms and the side chain of Arg8 of symmetry dimer 1 and a network of two water molecules linked it to Asn83. No hydrogen bond interactions were observed between SQV-B and symmetry related dimer 2. The minimal interactions of SQV-B with three symmetry related dimers suggested that it was likely a result of crystal packing. Interestingly, a second DRV binding site in a different location on the flap on one subunit was reported in HIV-1 PR_{V32I} and PR_{M46L} complexes[25] in the same space group and similar cell parameters. The SQV-B interacts closely with mutated Ile82 in PR_{1M}, which raises the question of whether SQV can bind to a similar second site in PR_2. The majority of residues contacting SQV-B are identical in PR_1 and PR_2 [Fig. 1(A)], however, the hydrogen bond interaction of SQV-B with the side chain of Glu34 cannot occur for Ala34 in PR_2, which lowers the probability of SQV binding at the equivalent site.

Comparison of PR-inhibitor structures

The interactions of the individual inhibitors were analyzed in their complexes with PR_{1M}, wild-type PR_1, and PR_2 to understand the structural effects of the three mutations. The following structures were chosen for the comparison: PR_1-DRV (2IEN at 1.30 Å resolution),[24] PR_1-APV (3NU3 at 1.02 Å resolution),[18] PR_1-SQV (2NMY at 1.10 Å resolution),[26] and PR_2-DRV (3EBZ at 1.20 Å resolution).[12] The PR_{1M} and PR_1 dimers are almost identical with small RMSDs of ~0.2 Å for the pairs of structures in the same space group and unit cell, whereas larger differences of 0.7–0.8 Å were apparent between structures with non-isomorphous unit cells. The largest difference of 1.1 Å was shown by PR_2-DRV and PR_2-APV structures compared with the corresponding PR_{1M} complexes, due in part to the different space groups. The majority of interactions with each inhibitor were conserved in the three enzymes. Therefore, the detailed structural analysis focusing on differences around residues 32, 47, and 82 is described separately for each inhibitor.

SQV complexes with PR_{1M} and PR_1

The PR_{1M} and PR_1 structures superimposed with the relatively large RMSD of 0.67 Å with the largest shifts of 2–3 Å for the surface residues 35–40. No suitable crystals were obtained for PR_2 with SQV. Comparison of the SQV interactions is complicated by the second SQV-B found in PR_{1M} (Fig. 3). SQV-A was bound within subsites S3 to S2′ of PR_{1M} and showed almost identical hydrogen bond interactions to those described for PR_1-SQV.[26] The minor exception was that SQV had a shorter hydrogen bond to the main chain carbonyl oxygen of Gly27 in PR_{1M} with a distance of 3.2 Å compared to the weaker interaction with longer separation of 3.6 Å for PR_1. A similar shorter interaction was described in the SQV complex with another mutant PR_{L76V},[27] however, the interaction in PR_{1M} may be influenced by the aromatic-aromatic interactions of the adjacent P1 and P3 groups of SQV-A with the quinoline rings of SQV-B [Fig. 3(A)].

The hydrophobic interactions at the sites of the three mutations are illustrated in Figure 4. The larger side chain of Ile32 added two hydrophobic interactions with the P2 Asn group of SQV-A in PR_{1M}, whereas both Ile47 and Val47 formed hydrophobic contacts with the P2 group [Fig. 4(A)]. Slight differences were seen in the other subunit resulting in one less hydrophobic contact of Ile32′ with the *t*-butyl group at P2′ of SQV-A in the mutant compared to the wild-type PR [Fig. 4(B)]. Ile82 in PR_{1M} formed more contacts with the P1′ decahydroisoquinoline ring compared to Val82 in PR_1 [Fig. 4(C)].

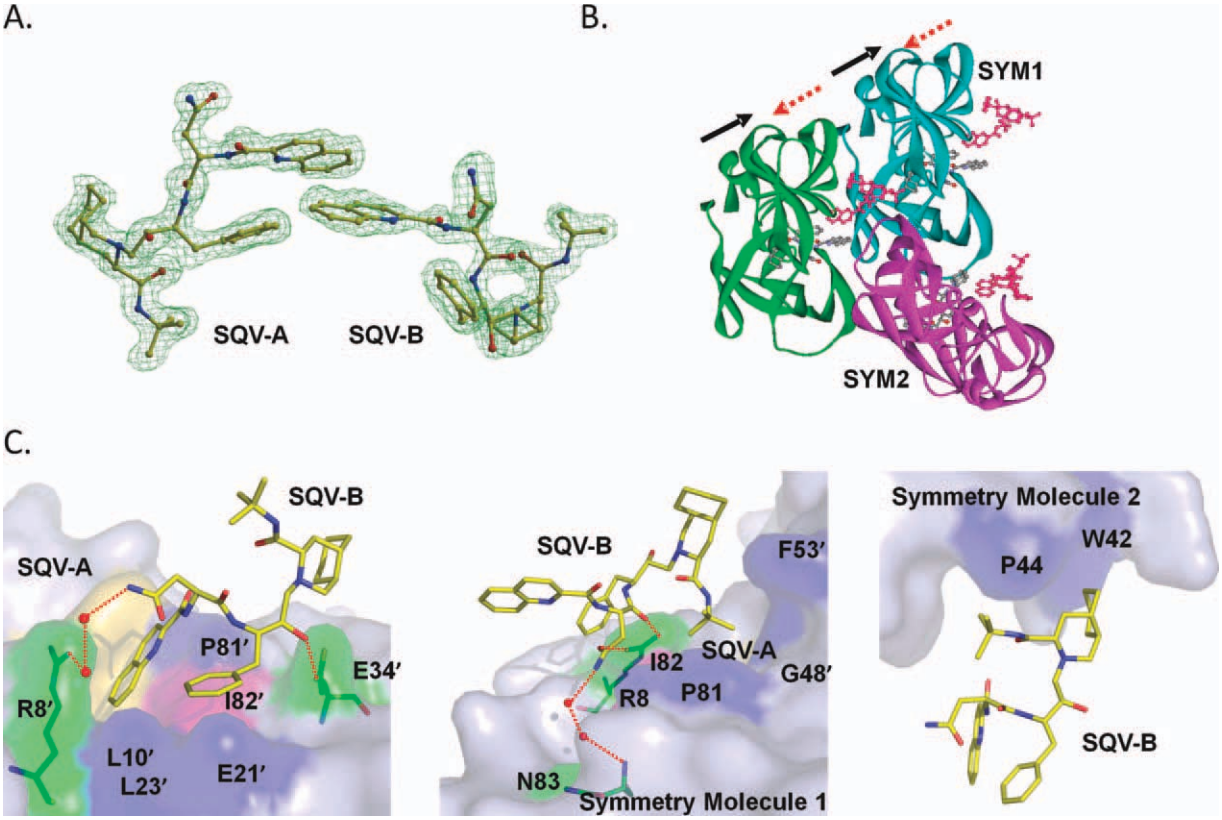

Figure 3. SQV-B in the extended binding site of PR_{1M}. A: Omit map for SQV-A and SQV-B. SQV-B interacts with SQV-A in an extension of the regular active site cavity. B: SQV-B molecule is surrounded by three PR_{1M} dimers in the crystal lattice, colored in green, cyan, and magenta. The SQV-A occupying the regular binding pocket is colored by atom type, whereas the extra SQV-B is shown in red. The arrows represent the alternating orientations of SQV-A and SQV-B molecules. C: SQV-B interactions with PR_{1M} dimer, symmetry-related dimer 1, and symmetry-related dimer 2. Mutated residues are in pink surface representation, SQV-A is in golden color, and the surfaces of the residues involved in polar or hydrophobic interactions are shown in green and blue, respectively. Water molecules are shown as red spheres. Hydrogen bonds are indicated by red dotted lines.
[Color figure can be viewed in the online issue, which is available at wileyonlinelibrary.com.]

In the other subunit, the methyl of the Ile82′ has shifted to make van der Waals contacts with the benzene ring at P1 of the second SQV-B [Fig. 3(D)]. The quinoline ring of SQV-A adjusted by about 15 degrees rotation to fit the SQV-B molecule. Pro81′ had shifted to interact with the P3 group of SQV-B while retaining hydrophobic contacts with the P1 and P3 groups of SQV-A [Fig. 4(D)]. Overall, the structural adjustment of the triple mutant to accommodate inhibitor binding was consistent with the similar inhibition constants observed for PR_{1M} and PR_1 with SQV of 0.24 and 0.11 n*M*, respectively.

DRV complexes with PR_{1M}, PR_1, and PR_2

DRV was bound in the active site cavity of PR_{1M} in two alternate conformations with relative occupancy of 0.55/0.45 in the active site cavity. This structure was very similar to that of wild type PR_1-DRV in the same space group with an overall RMSD on Cα atoms of only 0.16 Å. The PR_{1M}-DRV complex superimposed on PR_2-DRV (space group C2) with RMSD value of 1.1 Å, due to a large shift of 5–6 Å around residues 38–40 and 38′–40′, as described for comparison of the PR_1-DRV and PR_2-DRV crystal structures.[12] Notably, the PR_2-DRV crystal structure contained zinc ions and imidazole from the crystallization solution, although these solvent molecules were not close to the regions with large deviations.

The PR-DRV hydrogen bond interactions were essentially identical in the three enzymes. The minor exception was a slightly longer (3.4–3.5 Å) hydrogen bond interaction between one bis-THF oxygen of DRV and the amide of Asp30′ in PR_{1M} compared with distances of 3.1–3.3 Å in the other structures. Structural changes at the mutation sites are illustrated in Figure 5. Only the major conformation of DRV is shown for PR_1-DRV. Ile32 and 32′ in PR_{1M} had alternate conformations of the side chains with relative occupancies of 0.6/0.4 and 0.5/0.5, respectively. The side chains of Val32 and the minor conformation of Ile32 exhibited hydrophobic interactions with the aniline ring of DRV. Val47 in PR_{1M} had no contact with DRV, although Ile47 made two hydrophobic interactions with the aniline in PR_1 [Fig. 5(A)]. In the other subunit, the minor conformation of Ile32′ in PR_{1M} and Val32′ in PR_1 formed similar

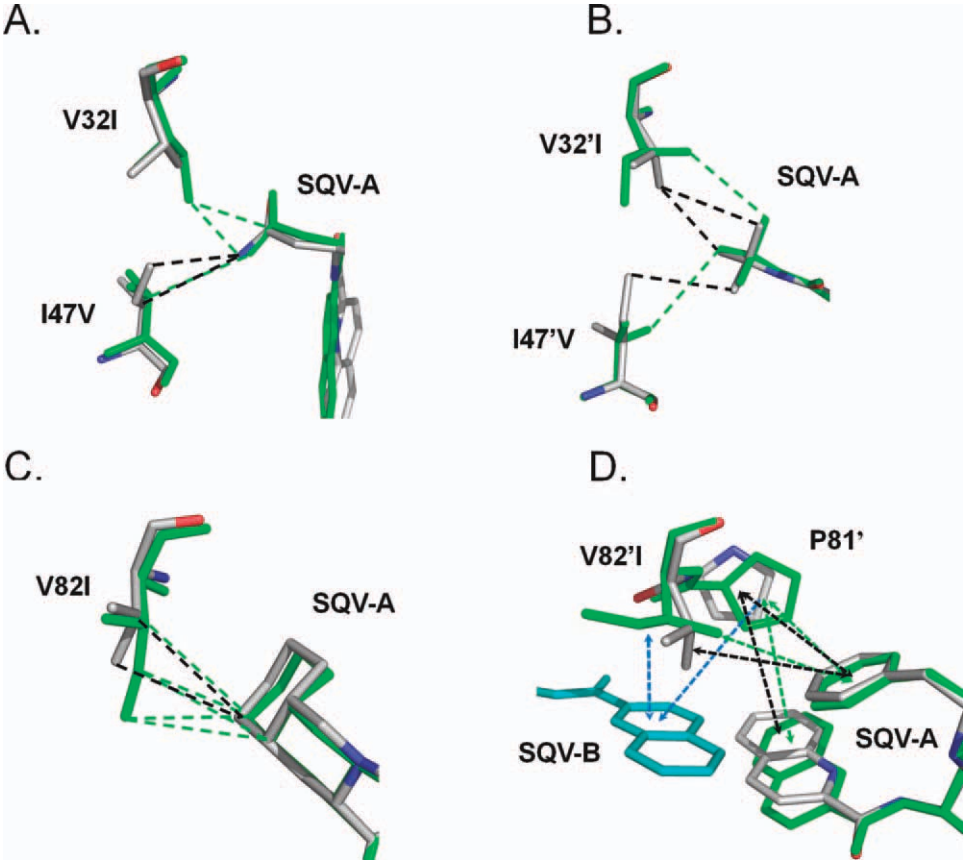

Figure 4. Comparison of PR_1 and PR_{1M} interactions with SQV. The PR_1 structure is colored by atom type, while that of the triple mutant is shown in green bonds. Only the major conformation is shown for SQV and protein residues with alternate conformation in the PR_1-SQV structure. SQV-A is the molecule bound in the regular active site cavity. Hydrophobic interactions (distances of 3.3–4.2 Å between non-hydrogen atoms) are indicated as dashed lines. Interactions with aromatic groups (CH...π) are indicated by dashed arrows. (A) Residues 32 and 47 of subunit A; (B) Residues 32′ and 47′ of subunit B; (C) Residue 82; (D) Residue 82′. SQV-B (cyan bonds) indicates the extra SQV molecule. [Color figure can be viewed in the online issue, which is available at wileyonlinelibrary.com.]

hydrophobic contacts with the bis-THF group, while the side chain of Val47′ rotated to make hydrophobic contacts with the bis-THF group unlike Ile47′ of PR_1 [Fig. 5(B)]. In comparison, the single mutant PR_{V32I}-DRV[25] showed similar interactions to those of the minor conformation of Ile32 in PR_{1M}. The side chain of Ile82 rotated to form comparable hydrophobic interactions with the P1 group of DRV as seen for Val82 in PR_1 [Fig. 5(C)]. Also, Ile82′ and Val82′ formed similar contacts with DRV in all structures.

In comparison of the PR_2 and PR_{1M}-DRV complexes, the side chain conformations of residues 32, 47, and 82 were preserved, except that the minor conformations of Ile32 and 32′ in the mutant most closely resembled the single conformation in PR_2. Ile32 formed CH...π interactions with the aniline ring of DRV in both complexes. The majority of the hydrophobic contacts for residues 32 and 82 were essentially identical in PR_1, PR_2, and PR_{1M}. Differences were observed in the DRV interactions of residue 47 [Fig. 5(B)]. Val47 had no hydrophobic interactions with the aniline of DRV in PR_2 and PR_{1M}, whereas two contacts were seen in PR_1. The opposite was seen for the other subunit, where Val47′ showed three van der Waals contacts with bis-THF in PR_2 and PR_{1M} and no contacts in PR_1. Overall, the slightly longer hydrogen bond interaction of the triple mutant with DRV was the only change that could help explain the 6-fold poorer inhibition of PR_{1M} compared to PR_2 and PR_1.

APV complexes with PR_{1M}, PR_1, and PR_2

The APV complex of PR_{1M} was very similar in overall conformation to PR_1-APV as shown by the low RMSD of 0.23 Å, whereas it had larger differences of 1.1 Å with the new structure of PR_2-APV solved in the C2 space group. APV was seen in a single orientation in PR_2 and PR_{1M}, although the aniline group in PR_{1M}-APV had two alternate conformations with an occupancy ratio of 0.6/0.4, as described for the PR_{V82A}-DRV structure.[24] Most of the PR_2 and PR_{1M} interactions with inhibitor were very similar to those of the major (0.7) occupancy conformation in the structure of PR_1 with APV,[18] with the exception of the interactions of the P2′ aniline group [Fig. 6(A)]. In PR_2 and PR_{1M}, Ile32 formed CH...π interactions with the

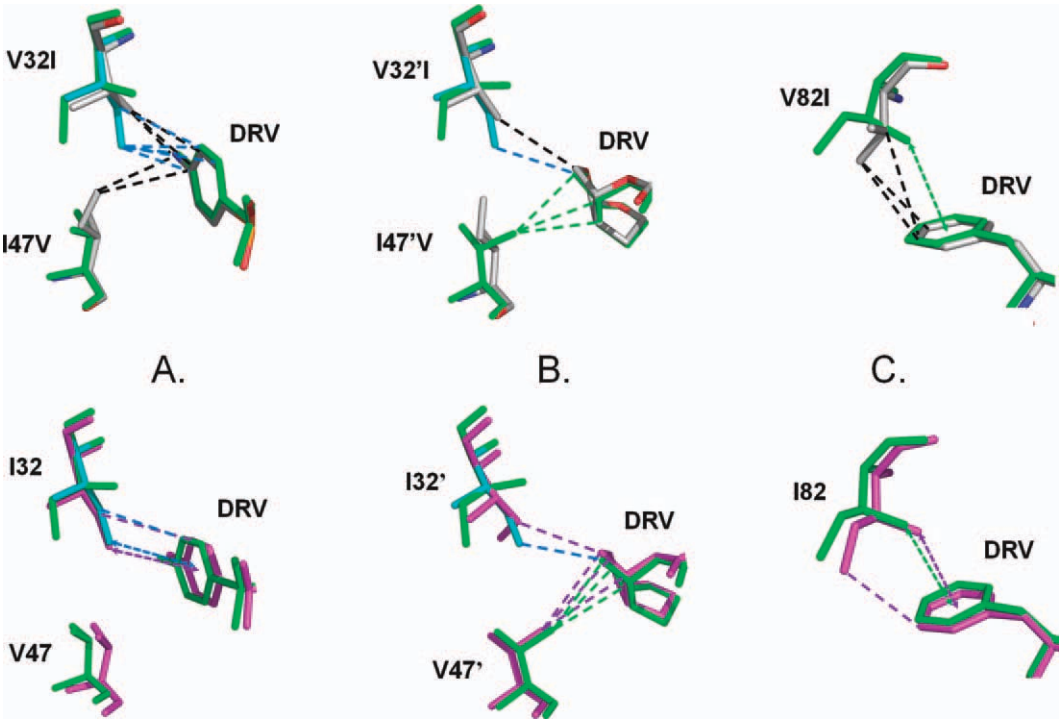

Figure 5. Structural comparison of DRV complexes with PR_{1M}, PR_1, and PR_2. The PR_1 structure is colored by atom type, PR_{1M} is shown in green bonds with the minor conformations of Ile32 and 32′ in cyan, and PR_2 is colored magenta. Only the major conformation of DRV is shown for PR_1-DRV. Hydrophobic interactions are indicated as dashed lines. CH. . .π interactions are indicated by dashed arrows. PR_{1M} is compared with PR_1 in the upper panels and with PR_2 in the lower panels. A: Residues 32 and 47 interactions with P2′ aniline of DRV; B: Residues 32′ and 47′ interactions with bis-THF at P2; and C: Residue 82 interactions with P1 of DRV. [Color figure can be viewed in the online issue, which is available at wileyonlinelibrary.com.]

aniline ring of APV, as occurred for the DRV complexes. In PR_{1M}-APV, the major conformation of the aniline group retained the hydrogen bond interactions seen in the wild type complex with distances of 3.0–3.1 Å, however, no van der Waals contacts were formed with Val47 unlike the favorable hydrophobic interactions with Ile47 seen in the wild type PR_1. The rotation of the minor conformation of the aniline restored favorable van der Waals interactions with Val47, concomitant with loss of the hydrogen bond interactions with the carbonyl oxygen and amide of Asp30 in PR_{1M} (interatomic distances of more than 4.0 Å). In the other subunit, the THF group of APV retained van der Waals contacts with residues 32′ and 47′ in the three structures [Fig. 6(B)]. The hydrophobic interactions of Ile32 with APV are similar in PR_2, PR_{1M} and the single mutant $PR_{V32I.}$[18] The side chain of Ile82 formed good hydrophobic interactions with the aromatic ring of APV similar to those in the DRV complexes [Fig. 5(C)]. Residue 82′ in the other subunit showed similar hydrophobic contacts with APV in all structures, although Ile82′ is closer to APV in the PR_2 complex [Fig. 6(C)]. In PR_{1M}-APV, the most significant differences arose from the alternate conformations of the aniline ring of APV, which were accompanied by the loss of hydrophobic contacts with Val47 for the major conformation and the loss of two hydrogen bonds for the minor conformation. The loss of these interactions with APV is likely to contribute to the 15-fold weaker inhibition by APV observed for the PR_{1M} compared with PR_1.

The crystal structure of PR_2-APV reveals notable changes in the hydrogen bond interactions of the aniline NH_2 with Asp30 where two interatomic distances are significantly lengthened by about 0.5 Å to 3.6 and 3.7 Å (Fig. 7), which is outside of the normal range of 2.6–3.2 Å for strong hydrogen bonds.[28] The elongated hydrogen bond is associated with a 1.2 Å shift of the carbonyl oxygen of Asp30 in the PR_2-APV complex relative to its position in the PR_1-APV complex. The altered interactions of the aniline group are consistent with the observed 19-fold weaker inhibition of PR_2 relative to PR_1.

Discussion

Recognition and selectivity in enzyme/substrate and enzyme/inhibitor systems are a complex combination of strong local effects and weaker, but still significant, distal effects. This is clearly demonstrated in our results where the three mutations in PR_{1M} which were chosen to mimic the inhibitor binding site of PR_2 changed the specificity and inhibition from the PR_1 toward the PR_2 values, but did not match them exactly. The relative k_{cat}/K_m values in

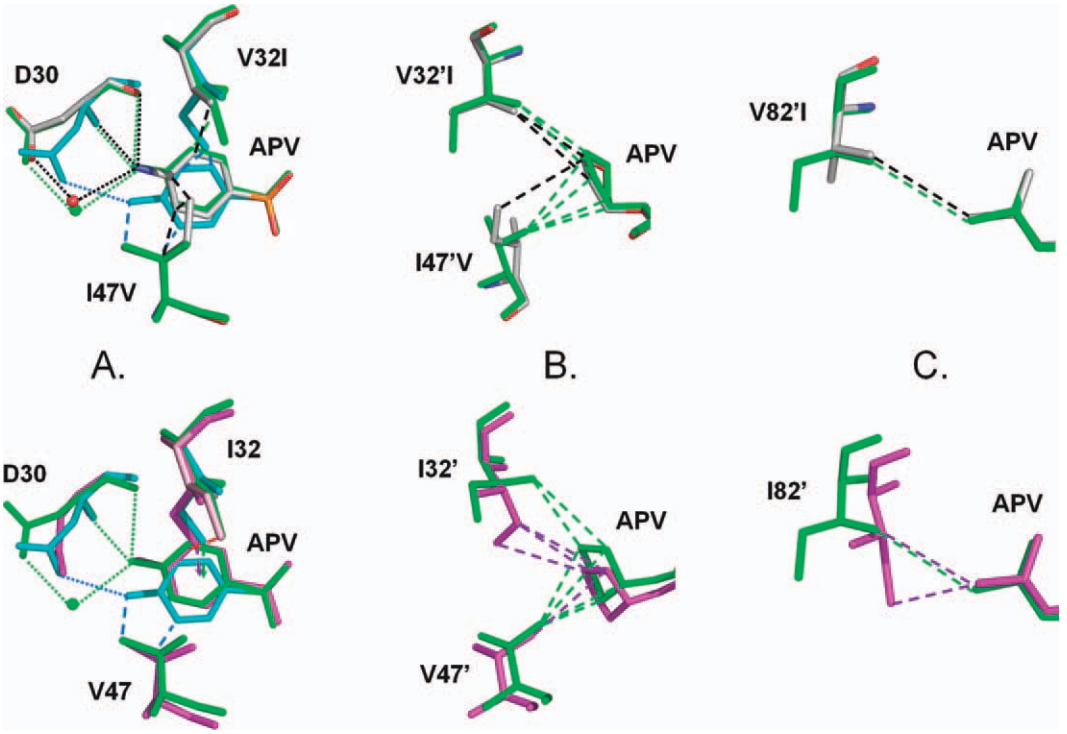

Figure 6. Comparison of PR_1, PR_2, and PR_{1M} interactions with APV. The PR_1 structure is colored by atom type, PR_{1M} is shown in green bonds with the minor conformations of Ile32 and 32′ in cyan, and PR_2 is colored magenta. Only the major (0.7 occupancy) conformation is shown for APV and PR_1 residues in the wild type complex. Hydrogen bond interactions are shown as dotted lines, hydrophobic interactions are indicated as dashed lines, and CH. . .π interactions are indicated by dashed arrows. A: Asp30, residues 32 and 47 interactions with aniline of APV. The aniline group and Asp30 have two alternate conformations in PR_{1M} -APV. The major conformations closely resemble the wild type structure with strong hydrogen bond interactions. The minor conformation (in cyan) has only one hydrogen bond and more hydrophobic interactions with Val47. B: Residue 32′ and 47′ interactions with the THF group of APV. C: Residue 82′ interactions with the P1′ group of APV. [Color figure can be viewed in the online issue, which is available at wileyonlinelibrary.com.]

Table I show that the specificity of the PR_{1M} enzyme roughly mirrors that of PR_2, and the K_i values in Table II reproduce the trend seen in PR_2, although the inhibition is measurably different for DRV. The biochemical similarities of PR_{1M} and PR_2 demonstrate the importance of residues 32, 47, and 82 for recognition. The differences between PR_{1M} and PR_2 are assumed to arise from distal effects due to over 50% difference in sequence (Fig. 1). Previously, differences in residues 31–37 were shown to make a major contribution to the inhibition and unusual mode of binding of a tripeptide analog in studies of chimeric enzymes.[17] In fact, residues 33–44 vary in sequence and conformation among different groups and subtypes of PR_1 although little effect on inhibition has been reported.[29–31]

Structurally, PR_{1M} resembles PR_1 more than PR_2. However, PR_{1M} and PR_2 share very similar side chain conformations for Ile32, Val47, and Ile82 reflecting the importance of local effects for recognition. Our crystallographic analysis of the weak inhibitor APV with PR_2 and the PR_{1M} mutant representing the inhibitor binding site of PR_2 helps explain the lower antiviral effectiveness of APV in HIV-2 infections compared to DRV or SQV. DRV and APV are chemically related and differ only in their P2 groups [Fig. 1(C)]. The bis-THF P2 group of DRV bears two oxygens and forms four hydrogen bonds with Asp29′ and Asp30′, while the THF group in APV forms only two hydrogen bonds[24](Fig. 7). Despite these differences, the P2 groups of APV and DRV retain similar interactions in PR_1 and PR_2. In contrast, the P2′ group at the opposite end of DRV maintains similar interactions in the enzymes, whereas the identical P2′ aniline of APV shows differences [Figs. 6(A) and 7]. The altered interactions of the P2′ aniline group of APV appear to reflect less stable anchoring of the P2 THF group relative to the larger bis-THF of DRV in the binding sites of PR_1 and PR_2

These new structures show how drug resistant mutations of V32I, I47V, and V82I can alter the interactions with the P2 and P2′ groups of inhibitors. The diminished interactions of APV with Asp30 and Val47 in PR_{1M} and PR_2 are consistent with the observed 15- and 19-fold weaker inhibition, respectively, relative to PR_1, and provide a structural explanation for the low antiviral potency on HIV-2 infections. In contrast, few structural changes were

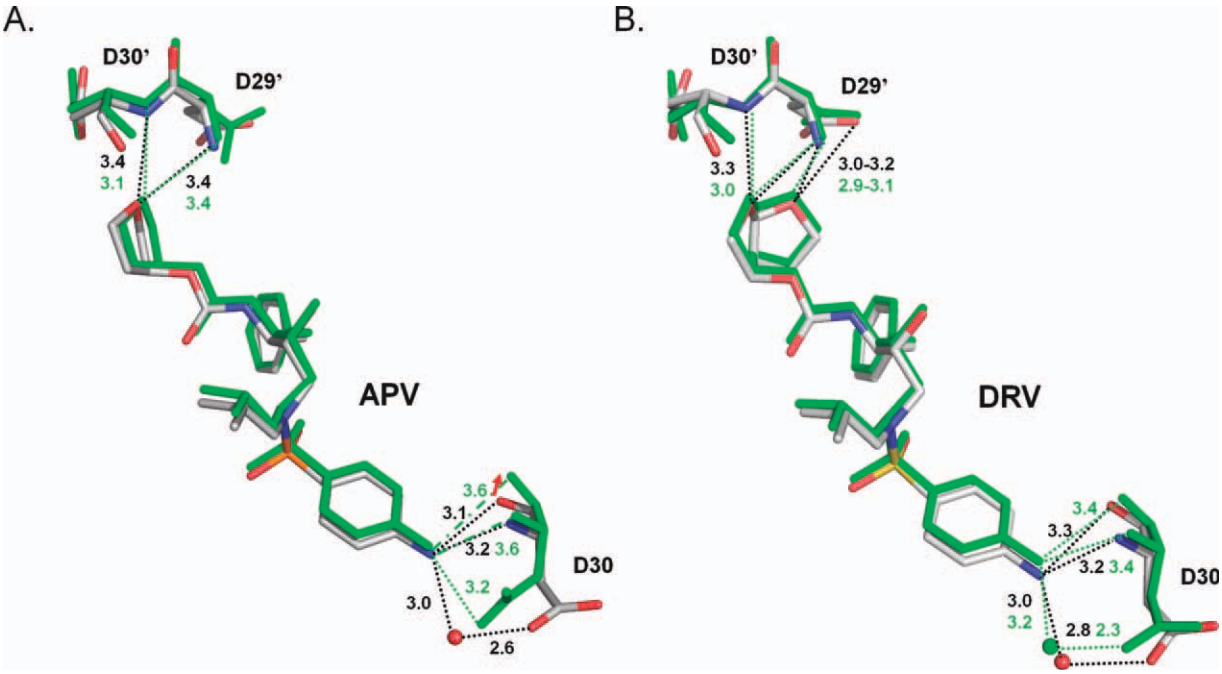

Figure 7. Hydrogen bond interactions of P2 and P2′ groups in PR_1 and PR_2 complexes with APV (A) and DRV (B). PR_1 complexes are shown in grey and PR_2 complexes in green bonds. The inhibitors are shown with Asp29 and 30. Dotted lines indicate hydrogen bonds with distances up to 3.4 Å, and broken lines indicate longer distances. The red arrow indicates the 1.2 Å shift of the carbonyl group of Asp30. [Color figure can be viewed in the online issue, which is available at wileyonlinelibrary.com.]

apparent for DRV and SQV complexes consistent with their sub-nanomolar inhibition of both enzymes and equivalent antiviral potency on HIV-1 and −2.[3] Therefore, this analysis suggests a strategy for improved inhibitors of HIV-2 and drug resistant HIV-1 by introducing P2 or P2′ groups with enhanced interactions in the S2 and S2′ subsites.

Materials and Methods

Preparation of proteases

The optimized HIV-1 PR clone with mutations Q7K, L33I, and L63I to diminish the autoproteolysis of the PR_1, as well as mutations C67A and C95A to prevent cysteine-thiol oxidation was used as the initial template for adding mutations.[32] This optimized PR_1 had almost identical kinetic parameters and stability as the mature PR. Plasmid DNA (pET11a, Novagen, Gibbstown, NJ) encoding PR_1 was utilized to construct mutant PR_{1M} with substitutions V32I/I47V/V82I by the Quick-Change mutagenesis kit (Stratagene, Santa Clara, CA). The PR_{1M} mutant was expressed in *Escherichia coli* BL21 (DE3) and the protein was purified from inclusion bodies as described.[33] The presence of the appropriate mutations was confirmed by DNA sequencing. PR_2 was prepared as described.[34]

Enzyme kinetic assays

Assays were performed at 37°C using purified PRs and chemically synthesized oligopeptides. The reaction was initiated by the mixing of 5 μL (0.05–8 μM) purified wild-type or mutant PR with 10 μL incubation buffer [0.5 *M* potassium phosphate buffer, pH 5.6, containing 10% glycerol, 2 m*M* ethylenediaminetetraacetic acid (EDTA), 10 m*M* dithiothreitol, 4 *M* NaCl] and 5 μL 0.5–7 m*M* substrate. The reaction mixture was incubated at 37°C for 1 h and terminated by the addition of 180 μL 1% trifluoroacetic acid. Substrates and the cleavage products were separated using a reversed-phase HPLC (High-performance liquid chromatography) method described previously.[32] Kinetic parameters were determined by fitting the data obtained at less than 20% substrate hydrolysis to the Michaelis–Menten equation using SigmaPlot 8.02 (San Jose, CA). The standard errors of the kinetic parameters were below 20%.

Active site titration of PR with SQV, APV, and DRV

The amount of active and correctly folded enzyme used in the assays was determined by active site titration using the PR_1 inhibitor DRV. Active site titrations were performed by using the HPLC method with substrate VSQLYPIVQ (peptide 4) as described,[35] except that 0.2 μL aliquot of the inhibitor (0–10 μM in dimethylsulfoxide) was added to the reaction mixture. K_i values were obtained from the IC_{50} values estimated from an inhibitor dose-response curve using the equation $K_i = (IC_{50} - [E]/2)/(1 + [S]/K_m)$, where $[E]$ and $[S]$ are the PR and substrate concentrations, respectively.[36]

Crystallographic analysis

Crystals were grown at room temperature by the hanging drop vapor diffusion method. The protein (about 3.5 mg/mL) was preincubated with the clinical inhibitors at a molar ratio of 1:5. Each crystallization drop contained 1 μL protein and 1 μL reservoir solution. Crystals of suitable size for diffraction were obtained within 1 week. PR_2-APV crystals grew from 1.5 *M* NaCl with 0.6 *M* imidazole/0.12 *M* zinc acetate buffer at pH 6. For PR_{1M}-SQV, 0.1 *M* sodium acetate buffer, pH 5.0, 0.4 *M* potassium chloride as precipitant; for PR_{1M}-APV, 0.1 *M* sodium citrate, phosphate buffer, pH 5.4, 4% dimethyl sulfoxide (DMSO) and 0.175 *M* potassium iodine as precipitant; For PR_{1M}-DRV, the crystal was grown from 0.1 *M* sodium acetate buffer, pH 4.6 and 2M NaCl as precipitant. Crystals were cryo-cooled in liquid nitrogen after soaking in 30% glycerol to prevent freezing.

X-ray diffraction data for all the complexes were collected on the SER-CAT 22ID beamline of the Advanced Photon Source, Argonne National Laboratory (Argonne, IL). Data were processed using HKL-2000.[37] The structures were solved by molecular replacement based on our published structures: PR_2-DRV (3EBZ), PR_1-SQV (2NMW), PR_{D30N}-GRL98065 (2QCI), and PR_1-DRV (2IEN) using AMoRe[38] in CCP4i.[39,40] The lowest resolution structure of PR_{1M}-SQV was refined using Refmac5 and isotropic B factors.[41] The other structures were refined by SHELX-97.[42] Structures were refitted using O[43] and COOT.[44] Alternate conformations for residues were modeled according to the electron density maps. Anisotropic B factors were refined and hydrogen atom positions were included in the last stage of refinement for the structures at better than 1.5 Å resolution. Structural figures were made using Bobscript[45,46] and PyMOL.[47]

Protein data bank accession numbers

The atomic coordinates and structure factors were deposited in the Protein Data Bank with accession codes: 3S56 for PR_{1M}-SQV, 3S54 for PR_{1M}-DRV ($P2_12_12$), 3S43 for PR_{1M}-APV, and 3S45 for PR_2-APV.

Acknowledgments

This research was authored, in whole or in part, by National Institutes of Health staff. This research was supported, in whole or in part, by the Hungarian Science and Research Fund (OTKA K68288, K101591), the Intramural Research Program of the NIDDK, National Institutes of Health (NIH), Intramural AIDS-Targeted Antiviral Program of the Office of the Director, NIH, and grants GM062920 (ITW) and GM53386 (AKG) from the NIH. The authors thank the staff at the SER-CAT beamline at the Advanced Photon Source, Argonne National Laboratory, for assistance during X-ray data collection. Use of the Advanced Photon Source was supported by the US Department of Energy, Office of Science, Office of Basic Energy Sciences, under Contract No. W-31-109-Eng-38.

References

1. AIDS at 30: Nations at the crossroads (2011) Geneva, Switzerland. http://www.unaids.org.
2. Peterson K, Jallow S, Rowland-Jones SL, de Silva TI (2011) Antiretroviral therapy for HIV-2 infection: recommendations for management in low-resource settings. AIDS Res Treat 2011:463704.
3. Menendez-Arias L, Tozser J (2008) HIV-1 protease inhibitors: effects on HIV-2 replication and resistance. Trends Pharmacol Sci 29:42–49.
4. Bock PJ, Markovitz DM (2001) Infection with HIV-2. AIDS 15 (Suppl 5):S35–S45.
5. Barin F, Cazein F, Lot F, Pillonel J, Brunet S, Thierry D, Damond F, Brun-Vezinet F, Desenclos JC, Semaille C (2007) Prevalence of HIV-2 and HIV-1 group O infections among new HIV diagnoses in France: 2003–2006. AIDS 21:2351–2353.
6. Maniar JK, Damond F, Kamath RR, Mandalia S, Surjushe A (2006) Antiretroviral drug-resistant HIV-2 infection—a new therapeutic dilemma. Int J STD AIDS 17:781–782.
7. Louis JM, Weber IT, Tozser J, Clore GM, Gronenborn AM (2000) HIV-1 protease: maturation, enzyme specificity, and drug resistance. Adv Pharmacol 49:111–146.
8. Berman HM, Westbrook J, Feng Z, Gilliland G, Bhat TN, Weissig H, Shindyalov IN, Bourne PE (2000) The Protein Data Bank. Nucleic Acids Res 28:235–242.
9. Brower ET, Bacha UM, Kawasaki Y, Freire E (2008) Inhibition of HIV-2 protease by HIV-1 protease inhibitors in clinical use. Chem Biol Drug Des 71:298–305.
10. Gustchina A, Weber IT (1991) Comparative analysis of the sequences and structures of HIV-1 and HIV-2 proteases. Proteins 10:325–339.
11. Chen Z, Li Y, Chen E, Hall DL, Darke PL, Culberson C, Shafer JA, Kuo LC (1994) Crystal structure at 1.9-A resolution of human immunodeficiency virus (HIV) II protease complexed with L-735,524, an orally bioavailable inhibitor of the HIV proteases. J Biol Chem 269: 26344–26348.
12. Kovalevsky AY, Louis JM, Aniana A, Ghosh AK, Weber IT (2008) Structural evidence for effectiveness of darunavir and two related antiviral inhibitors against HIV-2 protease. J Mol Biol 384:178–192.
13. Tozser J, Weber IT, Gustchina A, Blaha I, Copeland TD, Louis JM, Oroszlan S (1992) Kinetic and modeling studies of S3–S3′ subsites of HIV proteinases. Biochemistry 31:4793–4800.
14. Bagossi P, Sperka T, Feher A, Kadas J, Zahuczky G, Miklossy G, Boross P, Tozser J (2005) Amino acid preferences for a critical substrate binding subsite of retroviral proteases in type 1 cleavage sites. J Virol 79: 4213–4218.
15. Johnson VA, Brun-Vezinet F, Clotet B, Gunthard HF, Kuritzkes DR, Pillay D, Schapiro JM, Richman DD (2010) Update of the drug resistance mutations in HIV-1: December 2010. Top HIV Med 18:156–163.
16. Hoog SS, Towler EM, Zhao B, Doyle ML, Debouck C, Abdel-Meguid SS (1996) Human immunodeficiency virus protease ligand specificity conferred by residues outside of the active site cavity. Biochemistry 35: 10279–10286.
17. Swairjo MA, Towler EM, Debouck C, Abdel-Meguid SS (1998) Structural role of the 30's loop in determining

the ligand specificity of the human immunodeficiency virus protease. Biochemistry 37:10928–10936.
18. Shen CH, Wang YF, Kovalevsky AY, Harrison RW, Weber IT (2010) Amprenavir complexes with HIV-1 protease and its drug-resistant mutants altering hydrophobic clusters. FEBS J 277:3699–3714.
19. Desbois D, Roquebert B, Peytavin G, Damond F, Collin G, Benard A, Campa P, Matheron S, Chene G, Brun-Vezinet F, Descamps D (2008) In vitro phenotypic susceptibility of human immunodeficiency virus type 2 clinical isolates to protease inhibitors. Antimicrob Agents Chemother 52:1545–1548.
20. Witvrouw M, Pannecouque C, Switzer WM, Folks TM, De Clercq E, Heneine W (2004) Susceptibility of HIV-2, SIV and SHIV to various anti-HIV-1 compounds: implications for treatment and postexposure prophylaxis. Antivir Ther 9:57–65.
21. Rodes B, Sheldon J, Toro C, Jimenez V, Alvarez MA, Soriano V (2006) Susceptibility to protease inhibitors in HIV-2 primary isolates from patients failing antiretroviral therapy. J Antimicrob Chemother 57:709–713.
22. Ntemgwa M, Brenner BG, Oliveira M, Moisi D, Wainberg MA (2007) Natural polymorphisms in the human immunodeficiency virus type 2 protease can accelerate time to development of resistance to protease inhibitors. Antimicrob Agents Chemother 51:604–610.
23. Eizert H, Bander P, Bagossi P, Sperka T, Miklossy G, Boross P, Weber IT, Tozser J (2008) Amino acid preferences of retroviral proteases for amino-terminal positions in a type 1 cleavage site. J Virol 82:10111–10117.
24. Tie Y, Boross PI, Wang YF, Gaddis L, Hussain AK, Leshchenko S, Ghosh AK, Louis JM, Harrison RW, Weber IT (2004) High resolution crystal structures of HIV-1 protease with a potent non-peptide inhibitor (UIC-94017) active against multi-drug-resistant clinical strains. J Mol Biol 338:341–352.
25. Kovalevsky AY, Liu F, Leshchenko S, Ghosh AK, Louis JM, Harrison RW, Weber IT (2006) Ultra-high resolution crystal structure of HIV-1 protease mutant reveals two binding sites for clinical inhibitor TMC114. J Mol Biol 363:161–173.
26. Tie Y, Kovalevsky AY, Boross P, Wang YF, Ghosh AK, Tozser J, Harrison RW, Weber IT (2007) Atomic resolution crystal structures of HIV-1 protease and mutants V82A and I84V with saquinavir. Proteins 67:232–242.
27. Louis JM, Zhang Y, Sayer JM, Wang YF, Harrison RW, Weber IT (2011) The L76V drug resistance mutation decreases the dimer stability and rate of autoprocessing of HIV-1 protease by reducing internal hydrophobic contacts. Biochemistry 50:4786–95.
28. Sarkhel S, Desiraju GR (2004) N–H. . .O, O–H. . .O, and C–H. . .O hydrogen bonds in protein-ligand complexes: strong and weak interactions in molecular recognition. Proteins 54:247–259.
29. Sayer JM, Agniswamy J, Weber IT, Louis JM (2010) Autocatalytic maturation, physical/chemical properties, and crystal structure of group N HIV-1 protease: relevance to drug resistance. Protein Sci 19:2055–2072.
30. Vergne L, Peeters M, Mpoudi-Ngole E, Bourgeois A, Liegeois F, Toure-Kane C, Mboup S, Mulanga-Kabeya C, Saman E, Jourdan J, Reynes J, Delaporte E (2000) Genetic diversity of protease and reverse transcriptase sequences in non-subtype-B human immunodeficiency virus type 1 strains: evidence of many minor drug resistance mutations in treatment-naive patients. J Clin Microbiol 38:3919–3925.
31. Sanches M, Krauchenco S, Martins NH, Gustchina A, Wlodawer A, Polikarpov I (2007) Structural characterization of B and non-B subtypes of HIV-protease: insights into the natural susceptibility to drug resistance development. J Mol Biol 369:1029–1040.
32. Louis JM, Clore GM, Gronenborn AM (1999) Autoprocessing of HIV-1 protease is tightly coupled to protein folding. Nat Struct Biol 6:868–875.
33. Mahalingam B, Louis JM, Hung J, Harrison RW, Weber IT (2001) Structural implications of drug-resistant mutants of HIV-1 protease: high-resolution crystal structures of the mutant protease/substrate analogue complexes. Proteins 43:455–464.
34. Louis JM, Ishima R, Aniana A, Sayer JM (2009) Revealing the dimer dissociation and existence of a folded monomer of the mature HIV-2 protease. Protein Sci 18:2442–2453.
35. Tozser J, Blaha I, Copeland TD, Wondrak EM, Oroszlan S (1991a) Comparison of the HIV-1 and HIV-2 proteinases using oligopeptide substrates representing cleavage sites in Gag and Gag-Pol polyproteins. FEBS Lett 281:77–80.
36. Maibaum J, Rich DH (1988) Inhibition of porcine pepsin by two substrate analogues containing statine: the effect of histidine at the P2 subsite on the inhibition of aspartic proteinases. J Med Chem 31:625–629.
37. Otwinowski Z, Minor W (1997) Processing of X-ray diffraction data in oscillation mode. Methods Enzymology 276:307–326.
38. Navaza J (1994) A MoRe: an Automated Package for Molecular Replacement. Acta Crystallogr Sect A 50:157–163.
39. Collaborative Computational Project N (1994) The CCP4 suite: programs for protein crystallography. Acta Cryst D 50:760–763.
40. Potterton E, Briggs P, Turkenburg M, Dodson EA (2003) Graphical user interface to the CCP4 program suite. Acta Cryst D 59:1131–1137.
41. Murshudov GN, Vagin AA, Dodson EJ (1997) Refinement of macromolecular structures by the maximum-likelihood method. Acta Crystallogr D 53:240–255.
42. Sheldrick GM (2008) A short history of SHELX. Acta Crystallogr A 64:112–122.
43. Jones TA (2004) Interactive electron-density map interpretation: from INTER to O. Acta Crystallogr D Biol Crystallogr 60:2115–2125.
44. Emsley P, Lohkamp B, Scott WG, Cowtan K (2010) Features and development of Coot. Acta Crystallogr D Biol Crystallogr 66:486–501.
45. Esnouf RM (1997) An extensively modified version of MolScript that includes greatly enhanced coloring capabilities. J Mol Graph Model 15:132–134.
46. Esnouf RM (1999) Further additions to MolScript version 1.4, including reading and contouring of electron-density maps. Acta Cryst D55:938–940.
47. DeLano WL (2002) The PyMOL Molecular Graphics System. http://www.pymol.org.
48. Tozser J, Gustchina A, Weber IT, Blaha I, Wondrak EM, Oroszlan S (1991b) Studies on the role of the S4 substrate binding site of HIV proteinases. FEBS Lett 279:356–360.